Advances in Cylindrical Mathematical Absorber Reflection Suppression

S.F. Gregson[#1], A.C. Newell[#2], G.E. Hindman[#3], M.J. Carey[#4]

[#]*Nearfield Systems Incorporated*

19730 Magellan Drive, Torrance, CA 90502, USA

[1]*sgregson@nearfield.com*

[2]*anewell@nearfield.com*

[3]*ghindman@nearfield.com*

[4]*mcarey@nearfield.com*

***Abstract*— In many instances, reflections within antenna test ranges constitute the largest single component within the facility-level error budget [1]. For some time, a frequency domain measurement and post-processing technique named Mathematical Absorber Reflection Suppression (MARS) has been successfully used to reduce range multi-path effects within spherical near-field and far-field antenna measurement systems [2, 3, 4]. More recently, a related technique has been developed for use with cylindrical near-field antenna measurement systems [5, 6]. This paper provides an introduction to the measurement technique and novel probe pattern corrected near-field to far-field transform algorithm. It then presents the most recent results of an ongoing validation campaign detailing a number of the most recent advances which are found to yield improvements comparable to those attained with the corresponding spherical MARS technique. The results are discussed and conclusions presented.**

I. Introduction

Since its inception, the cylindrical near-field (CNF) antenna measurement technique [7, 8, 9] has developed into a powerful method for accurately and precisely characterising the performance of medium to high gain antennas at reduced range lengths. The technique is perhaps best suited to higher gain antennas or those radiators possessing a commensurate cylindrical radiating structure corresponding to a fan-beam far-field antenna pattern function. The appeal of the technique for the characterisation of broad beam antennas renders the results susceptible to the deleterious effects of range multi-path which is a consequence of the relatively high field intensities that can illuminate the walls of the chamber. Thus, as the absorbent material which is used to line the chamber is in general not perfectly matched to illuminating fields for all directions, polarisations and frequencies, the resulting scattering can influence significantly the measurements taken therein. Whilst considerable effort, ingenuity and resourcefulness have been devoted to improving the quality of measurements taken in spherical near-field, far-field, and compact antenna test ranges (CATR), it is only relatively recently that cylindrical near-field facilities have received similar attention [5, 6].

MARS is a sophisticated measurement and post-processing technique that has been developed to improve the quality of measurements taken in anechoic chambers [2, 3, 4]. The success of this technique has been attested to across a wide range of frequencies and on numerous different antenna types. The general MARS principle involves a measurement and post-processing technique that analyses the measured data before utilising a special filtering process to suppress undesirable scattered fields. This frequency-domain technique is completely general requiring only a minimum amount of information about the AUT and measurement configuration. The analogous cylindrical MARS (C-MARS) technique has been shown to be highly effective in correcting measurements taken in multi-path rich environments, of both high and low gain radiators, and has been found to provide significant levels of isolation from contaminants.

II. Overview of Measurement and Transformation Techniques

It is well known that the electromagnetic fields outside an arbitrary test antenna radiating into free space can be expanded onto a set of elementary orthogonal cylindrical mode coefficients (CMCs) and that these modes and coefficients can then be used to obtain the electric and magnetic fields everywhere in space outside of a conceptual right circular cylindrical surface which encloses that radiator using the principle of linear superposition [7, 8, 9].

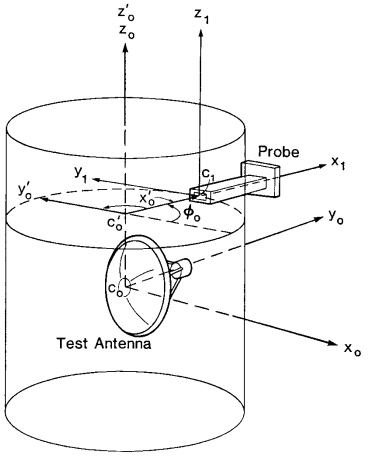

Fig. 1 Schematic of AUT and probe cylindrical co-ordinate systems. C_0 is AUT centred system, C_0' and C_0'' are AUT centred probe systems.

The relevant cylindrical measurement co-ordinate system is presented in Fig 1. When expressed in component from, and when assuming an infinitesimal Hertzian dipole is employed as a near-field probe (this assumption is not an inherent limitation of the technique and is merely introduced to simplify the pedagogy), the two sets of orthogonal CMCs $B_n^1(\gamma), B_n^2(\gamma)$ can be obtained from [5, 9] where the symbols have their usual meanings,

$$B_n^1(\gamma) = \frac{-1}{4\pi^2\kappa^3 H_n'^{(1)}(\kappa\rho_0)} \int_{-\infty}^{\infty}\int_0^{2\pi} \left[\frac{n\gamma}{\rho_0} E_z(\rho_0,\phi,z) + \kappa^2 E_\phi(\rho_0,\phi,z) \right] e^{-j(n\phi+\gamma z)} d\phi dz \quad (1)$$

$$B_n^2(\gamma) = \frac{k_0}{4\pi^2\kappa^2 H_n^{(1)}(\kappa\rho_0)} \int_{-\infty}^{\infty}\int_0^{2\pi} [E_z(\rho_0,\phi,z)] e^{-j(n\phi+\gamma z)} d\phi dz \quad (2)$$

CMCs are complex quantities that are functions of the polarization index s, the ϕ index n and the Fourier variable γ. In practice CMCs are determined from the measured data in a very efficient manner through the use of a two-dimensional fast Fourier transform (FFT). Once obtained, these mode coefficients are corrected for the spatial filtering properties of the near-field probe to determine the true AUT transmitting CMCs. Then, a highly efficient one-dimensional FFT based summation process is utilised to obtain the asymptotic far electric field using [5, 9],

$$E_\theta(r\to\infty,\theta,\phi) = 2jk_0 \sin\theta \sum_{n=-\infty}^{\infty} (-j)^n B_n^2(\gamma) e^{jn\phi} \quad (3)$$

$$E_\phi(r\to\infty,\theta,\phi) = -2k_0 \sin\theta \sum_{n=-\infty}^{\infty} (-j)^n B_n^1(\gamma) e^{jn\phi} \quad (4)$$

Thus, asymptotic far-field parameters providing pattern, polarisation, gain, *etc.*, information are obtained from the electric field and the plane-wave condition. As the z-axis is of only a finite length, the AUT is typically installed within the positioning system using an equatorial mode mounting so that truncation is minimised. The resulting pattern data is naturally tabulated on a regular azimuth over elevation co-ordinate system and resolved onto a Ludwig II, azimuth over elevation polarisation basis. Thus, it is possible to compute the complete electromagnetic six-vector everywhere in space outside the conceptual coaxial cylinder of minimum radius that circumscribes the majority of the current sources which is coaxial with the sampling cylinder and is formed from the intersection of linear and rotational axes.

As only propagating modes can contribute to the far-field pattern, the Fourier variable γ can be limited to $\pm k_0$ as these represent the highest order propagating mode coefficients. This therefore also places a limit on the sample spacing in the linear axis that is required to obtain data that is free from aliasing with the sample spacing δ_z (*i.e.* the resolution) in the linear axis is determined from the maximum value of γ, as $\delta_z = \lambda/2$ where λ is used to denote the free-space wavelength. This then is just the Nyquist criteria.

Typically, an antenna is installed within a near-, or far-field facility such that it is displaced in space as little as possible during the course of a measurement. As range multi-path tend to disturb the fields illuminating the test antenna, the purpose of this strategy is to insure that the field illuminating the test antenna changes as little as possible during the course of the acquisition. This also minimises the maximum radial extent (MRE) and as a consequence of the sampling theorem maximises the sample spacing in the angular axis as [5, 10, 11],

$$\delta\phi = 2\pi/(2N+1) \quad (5)$$

Where,

$$N = \text{ceil}(k_0 r_t) + n_1 \quad (6)$$

Here, ceil is used to denote a function that rounds to the nearest integer towards positive infinity, n_1 is a positive integer that depends upon the accuracy required (*e.g.* $n_1 = 10$), N is the maximum cylindrical mode index required to represent the radiated fields, r_t is the MRE and $\delta\phi$ is the sample spacing in the angular axis. However, the MARS measurement technique adopts a fundamentally unconventional strategy whereby the test antenna is deliberately displaced from the centre of rotation. This has the effect of making the differences in the illuminating field far more pronounced than would ordinarily be the case, and it is exactly this greater differentiation that makes their identification and subsequent extraction viable. As the MRE is increased, from inspection of equations 5 and 6 it is clear that a larger number of CMCs are required to represent the field and that this results in a decrease in the angular sample spacing and an increase in the amount of measured data that is required to be taken.

Once the probe corrected electric far-fields have been determined, the phase reference can be displaced by means of the application of a simple differential phase change [11], *i.e.*,

$$\underline{E}_t(r\to\infty,\theta,\phi) = \underline{E}(r\to\infty,\theta,\phi) e^{j\underline{k}_0\cdot\underline{r}} \quad (7)$$

Here, $\underline{r}$ denotes the displacement vector between the centre of the measurement co-ordinate system and the centre of the aperture of the AUT. Thus, assuming that Δx, Δy and Δz are the AUT displacements in the x-, y- and z-axes respectively it can be shown that,

$$\underline{k}_0 \cdot \underline{r} = k_0(-\Delta x \sin Az \cos El + \Delta y \cos Az \cos El + \Delta z \sin El) \quad (8)$$

Crucially, whilst in principle all we have done is to conceptually, *i.e.* mathematically, translate the AUT back to the origin of the measurement co-ordinate system, from the sampling theorem it is clear that this has the corresponding effect of reducing the number and order of CMCs that are required to accurately represent the radiated field. The reduced set of translated CMCs can be efficiently computed through the use of an inverse one-dimensional FFT from an inversion of equations 3 and 4 [5]. Thus, any CMCs corresponding to fields that are exterior to this reduced region of space can be safely filtered out using a band-pass brick-wall filter function without compromising the integrity of the underlying antenna pattern function. When expressed mathematically the mode filter becomes,

$$B_n^s(\gamma)\big|_{s=1,2} = \begin{cases} B_n^s(\gamma) & n^2 + (\gamma r_{t0})^2 \le (k_0 r_{t0})^2 \\ 0 & \text{elsewhere} \end{cases} \quad (9)$$

Here, s denotes the polarisation index of the CMCs and r_{t0} the optimum MRE, rather than the actual MRE as taken from the near-field measurement where $r_t > r_{t0}$. The mode cut-off is based on the fact that antenna related modes above a certain index number are exponentially attenuated and do not

contribute to the far-fields. Thus in effect, the mode cut off is determined by the physical dimensions of the AUT. The final step in the processing is to reconstruct the filtered far-field antenna pattern from equations 3 and 4. Whilst a certain degree of effort is required to calculate the CMCs from the far-field pattern, and then reconstruct the far-field pattern from the filtered set of CMCs, as neither of these operations requires the computation of Hankel functions (or their derivatives), and since the transforms are evaluated with the efficient FFT algorithm, these operations are both robust and very cost effective in terms of computational effort, especially when compared to other alternative strategies. In order that range multi-path can be effectively suppressed, previously, it has been shown that the magnitude of the displacement in the *y*-axis (*i.e.* at a normal to the aperture plane of the AUT) should be greater than the diameter of the conceptual optimum MRE [5]. Thus, providing the displacement is applied in the *y*-axis this holds when,

$$|r| > 2r_{t0} \tag{10}$$

In understanding the nature of the C-MARS technique it is beneficial to illustrate the effect of displacing a given AUT within the cylindrical measurement co-ordinate system on the CMCs. Figs 2 – 5 contain false-colour plots of the amplitudes of the CMCs modes for $s = 1$, *i.e.* B^1, before (Fig 2) and after applying 0.3084 m (12") displacements successively in each of the Cartesian *x*-, *y*- and *z*- axes as defined in Fig 1.

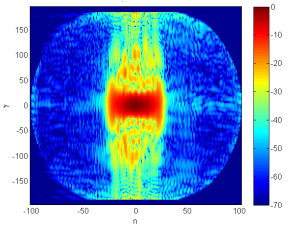

Fig. 2 AUT located at origin (Baseline – conventional case)

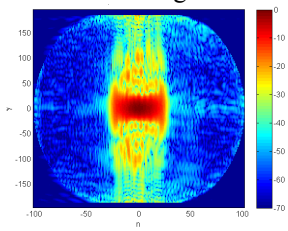

Fig. 3 AUT displaced in *z*-axis (Not used for C-MARS)

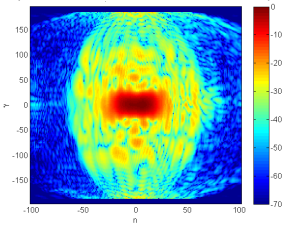

Fig. 4 AUT displaced in *y*-axis (Conventional C-MARS offset)

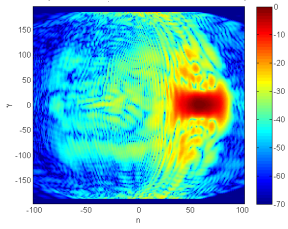

Fig. 5 AUT displaced in *x*-axis (Alternative C-MARS offset)

Here, it is clear that as the antenna is displaced in the *z*-axis there is no change in the amplitude of the CMCs (although not shown, a phase taper *is* introduced which is a function of γ). Conversely, when displacing the AUT in the *y*-axis it is clear that the CMCs associated with the AUT are distributed across a broader range of modes. A similar effect is also observed when the AUT is translated in the *x*-axis, however here the modes remain broadly similarly distributed although they are centred about a higher order mode index. Thus, when taking C-MARS measurements, the object of the experimental setup is to acquire data similar to either Fig 4, or Fig 5, and then to reconstruct the mode pattern of Fig 2. Although the magnitudes of the displacements were the same in each of these cases, the effect that this has on the MRE (and correspondingly the highest order mode index) do differ. A displacement in the *z*-axis has no effect on the MRE. A displacement in the *x*-axis increases the MRE such that $MRE_t = MRE + \Delta x$. A displacement in the *y*-axis can yield a MRE_t somewhere between these two cases. This slight difference is observable from inspection of the mode plots.

III. Measured Results

In order that the extended generalised C-MARS measurement and post-processing technique could be verified (*i.e.* for the case when the AUT is offset in the *x*- and/or *y*-axes) an NSI-200V-3x3 combination planar/ cylindrical/ spherical (PCS) system was used to test a 12.0" wide by 11.6" high x-band slotted waveguide planar array antenna in a partially absorber lined chamber. A rectangular metal reflecting plate was introduced into the chamber to enable the amount of scattering to be significantly increased in a known, controllable manner. This system is shown in Fig. 6.

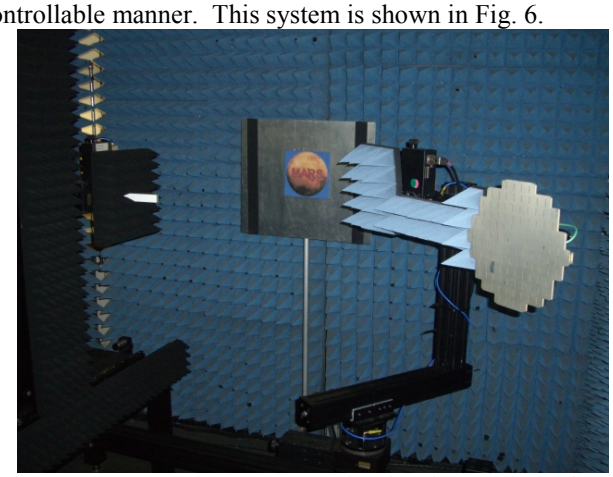

Fig. 6 NSI-200V-3x3-PCS System measuring slotted array antenna shown offset in the range *x*-axis.

The first measurement was a baseline where the AUT was placed at $x = y = z = 0$. Although, the MRE could have been as small as 6", a larger MRE was used so as to be equal to future measurements where the AUT was offset. Baseline scans were taken without the reflecting plate and then with the plate in the plus and minus *x* positions. The C-MARS technique was then verified against a second set of scans which were performed with the AUT offset at various positions of *x* and with the reflecting plate absorbed or offset in *x* at +/- 42". Fig 7 contains a false-colour plot of the amplitudes of the CMC's modes for $s = 1$ resulting from a scan taken with the AUT offset by 12" and a reflecting plate positioned at $x = 42$". Inspection of Fig 7 clearly shows that the energy from the AUT and the reflecting plate are superimposed on one another approximately about mode index $n = 60$. Once the AUT has been mathematically translated back to the origin of the "conceptual" measurement co-ordinate system, the resulting CMC plot can be found presented in Fig 8. Inspection of Fig 8 reveals that those modes associated with the AUT are tightly distributed and

centred about mode index n = 0 and as such are therefore separated (and distinct) from those modes that are associated with the reflecting plate which are still centred about the higher order n = 60 mode index. A conceptual minimum cylinder that would enclose the majority of the antenna's current sources (drawn as a black ellipse in Fig 8) should contain energy primarily resulting from just the AUT allows the filtering of all the higher order modes outside the ellipse that would not be emanating from the AUT. All higher order modes can therefore be filtered out using equation 9.

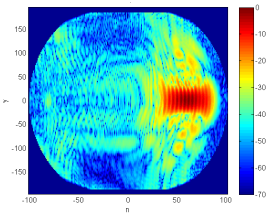

Fig. 7 Displaced AUT with reflecting plate

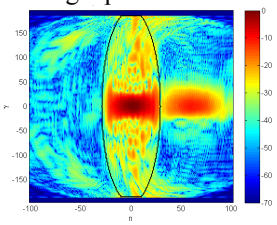

Fig. 8 AUT Mathematically translated back to the origin

The far-field plots before (Fig. 9) and after C-MARS filter (Fig. 10) are very encouraging as they show an almost complete suppression of the scattered energy which is caused by the insertion of the reflecting plate. Additionally, the high frequency ripple that was evident in the unfiltered results is clearly absent in the processed result. Clearly, C-MARS can not distinguish between modes associated with the reflecting plate, and those associated with unaccounted reflections due to imperfections in the partially absorber lined chamber used for these tests which will also be suppressed. Thus, for the first time, C-MARS processing has been demonstrated for the case where the displacement lies within the aperture plane of the AUT and is at a normal to the axis of rotation. In all previous cases, the displacement was applied along a vector that was at a normal to the antenna aperture plane.

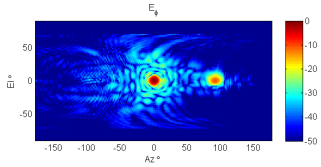

Fig. 9 No C-MARS processing

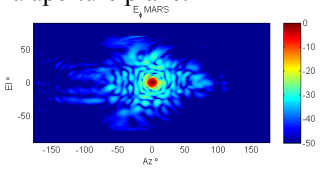

Fig. 10 With C-MARS processing

These patterns do however suffer from a significant amount of truncation in the elevation plane and the pattern data at larger angles is unreliable as a result of the onset of the first order truncation effect which is due to the large measurement radius and the comparatively short travel of the linear scan axis of 3'. As the AUT is offset in the x-axis, the truncation in the elevation axis is also a function of the azimuth angle. This, in combination with the asymmetric blockage which is presented by the fixture that was used to mount and displace the AUT in the x-axis is responsible for the asymmetrical (in the azimuth axis) far-field antenna patterns that are observed here. These tests also revealed that the magnitude of the x-axis displacement that is required to suppress the reflections, in certain specific cases, was required to be larger than that required for y-axis displacement. Thus, the additional amount of near-field data that this therefore requires, when combined with the extra blockage presented by the additional mechanical support equipment perhaps indicates that the conventional y-axis displacement is the preferable measurement configuration.

A common and very simple technique to identify or estimate reflection levels in a spherical test range is to make a comparison of a theta cut with the AUT phi angle changed between 0° and 180°. For a correctly aligned measurement system, the differences in the patterns are due to the range reflections and will give a preliminary estimate of expected error signal level for the far-field patterns. An analogous measurement can be made in the cylindrical case where the AUT is acquired in the same two opposing orientations. These tests would thereby allow the "real-world" utility of the C-MARS technique to be verified. Thus, the slotted waveguide planar array antenna was acquired once the "right way up", and again "up side down" after it had been rotated about its boresight axis by 180°. The resulting measurements were transformed to the far-field and can be found presented in the form of a false-colour plot in the antenna co-ordinate system. The necessary transformation, *i.e.* 180° rotation, from the range co-ordinate system to the antenna co-ordinate system was implemented by applying a vector isometric rotation to one of the far-field patterns [11]. Thus when comparing the 0° and 180° patterns, the only differences in the patterns should result from range multi-path effects as the AUT is assumed to be time invariant, *i.e.* it is taken to be both gravitationally and thermally insensitive.

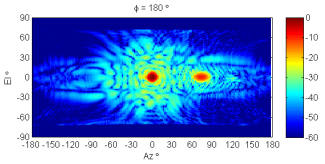

Fig. 11 AUT "right way up" without C-MARS processing

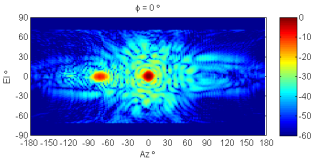

Fig. 12 AUT "up side down" without C-MARS processing

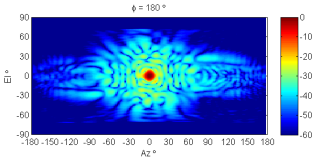

Fig. 13 AUT "right way up" with C-MARS processing

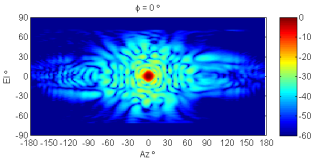

Fig. 14 AUT "up side down" with C-MARS processing

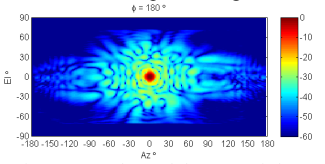

Fig. 15 Truth model AUT "right way up" with C-MARS processing

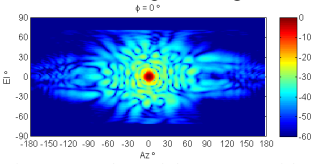

Fig. 16 Truth model AUT "up side down" with C-MARS processing

Here, all of the measurements employed a y-axis displacement for the purposes of enabling C-MARS processing. A comparison of Fig 11 and Fig 12 reveals that when plotted in the antenna co-ordinate system, as expected, the spectral flash of the reflecting plate has appeared to changed sides between the respective measurements. All other range reflection effects will have similarly changed positions although their effects are less immediately apparent. Fig 13 and Fig 14 contain equivalent patterns with the C-MARS processing having been applied. From inspection, the

large spectral flash lobe can be seen to have been effectively suppressed with the agreement between the respective patterns being very encouraging. As this is an extreme, perhaps unrealistic example, the rectangular metal reflecting plate was removed from the range and the measurements repeated. These data were C-MARS processed using exactly the same data processing chain. The results of this can be found presented in Fig 15 and Fig 16. Again, these patterns are found to be in very good agreement with the equivalent multi-path contaminated C-MARS processed patterns, in the forward hemisphere and even in much of the rear hemisphere where the field intensities are lower. Thus, at least for a range scattering perspective, these figures can reasonably be taken to represent the "truth" model against which the other results can be measured. The higher Equivalent Multi-Path Level (EMPL) [11] values near boresight are principally an artefact of imperfections in the alignment in elevation that exists between the two measurements (the application of a 180° rotation will double the apparent impact of any alignment error).

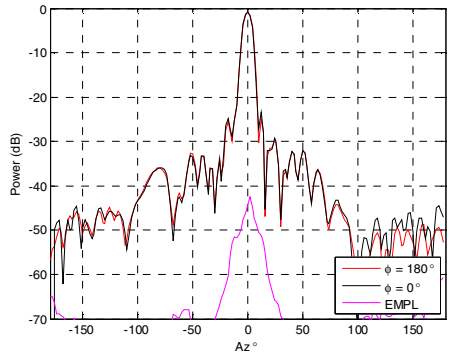

Fig. 17 Comparison of C-MARS corrected repeat reference measurements verifying validity of antenna pattern "truth" model.

The degree of agreement attained is clearly very encouraging leading to the assertion that with C-MARS processing high quality antenna measurements can be taken even in scattering environments that are less than perfect. Please note that these measurements were not taken in NSI's permanent antenna test service facilities but rather in a small temporary enclosure.

IV. Conclusions & Future Work

Cylindrical MARS processing can be used with a good degree of confidence since all the steps in the measurement and analysis are consistent with the well established principles of the cylindrical near-field theory and measurement techniques, and all comparisons have proved overwhelmingly positive. The offset of the AUT and the resulting smaller data point spacing are valid if the spacing satisfies the sampling criteria. The translation of the far-field pattern to the origin with the phase shift is rigorous. The selection of the mode cut-off for the translated pattern is based on the physical dimensions of the AUT and its translated location. The recommended mode cut-off is calculated from the AUT dimensions but can be modified by the user if the cylindrical mode plots, *e.g.* Fig 8, suggest a different cut-off is required. The results of the C-MARS processing will always reduce, but not entirely eliminate, the effective of scattering. The final result with C-MARS can be degraded if the sampling of the near-field data is too large, or the mode filter is too small, but this is also true for regular cylindrical processing. Importantly, both of these parameters are controlled by the user and must be correctly specified.

NSI has developed and validated a novel technique to suppress reflections in cylindrical near-field ranges which is implemented efficiently by means of the FFT algorithm. The technique is entirely general and can be used to achieve acceptable results with use of minimal absorber or even with no anechoic chamber. It can also improve the reflection levels in a traditional anechoic chamber by 10 dB or more, allowing improved accuracy as well as the ability to use existing chambers down to lower frequencies than the absorber might otherwise indicate.

NSI has successfully developed reflection suppression techniques that are highly effective at improving measurements taken in spherical and now cylindrical antenna measurement ranges. It should be noted however that this paper recounts the progress of an ongoing research study. Consequently, several issues remain to be addressed. Of the planned future work, obtaining experimental verification of the success of the C-MARS filtering algorithm (which essentially operates on a single cut-by-cut basis) with conventional, single-cut, direct far-field measurements is perhaps of greatest interest and utility.

References

[1] A.C. Newell, "Error Analysis Techniques for Planar Near-field Measurements", IEEE Transactions on Antennas and Propagation, vol. AP-36, pp. 754-768, June 1988.

[2] G.E. Hindman, A.C. Newell, "Reflection Suppression in a large spherical near-field range", AMTA 27th Annual Meeting & Symposium, Newport, RI, October. 2005.

[3] G.E. Hindman, A.C. Newell, "Reflection Suppression To Improve Anechoic Chamber Performance", AMTA Europe 2006, Munch, Germany, March 2006.

[4] G.E. Hindman, A.C. Newell, "Mission To MARS – In Search of Antenna Pattern Craters", AMTA 28th Annual Meeting & Symposium, St. Louis, MO, November 2007.

[5] S.F. Gregson, A.C. Newell, G.E. Hindman, "Reflection Suppression In Cylindrical Near-Field Antenna Measurement Systems – Cylindrical MARS", AMTA 31st Annual Meeting & Symposium, Salt Lake City, UT, November 2009.

[6] S.F. Gregson, A.C. Newell, G.E. Hindman, "Reflection Suppression In Cylindrical Near-Field Measurements of Electrically Small Antennas", Loughborough Antennas & Propagation Conference, November, 2009.

[7] J. Brown and E.V. Jull, "The Prediction of Aerial Radiation Patterns From Near-Field Measurements," Proc. of the Institute of Electrical Engineers, Vol 108-B, Nov. 1961, pp. 635-644.

[8] W.M. Leach, D.T. Paris, "Probe Compensated Near-Field Measurements On A Cylinder", IEEE Trans. on Antennas and Propagation, AP-21, No. 4, July 1973, pp. 435-444.

[9] A.D. Yaghjian, "Near-Field Antenna Measurements On a Cylindrical Surface: A Source Scattering Matrix Formulation", NBS Technical Note 696, 1977.

[10] J.E. Hansen (ed.), "Spherical Near-Field Antenna Measurements", The Institution of Engineering and Technology, UK, Peter Peregrinus Ltd., 1988.

[11] S.F. Gregson, J. McCormick, C.G. Parini, "Principles of Planar Near-Field Antenna Measurements", The Institution of Engineering and Technology, UK, 2007.